Modeling the Impact of Granular Flow against an Obstacle

Adel Albaba[1,2], Stéphane Lambert[1], François Nicot[1], and Bruno Chareyre[2]

[1] Irstea, UR ETGR, 2 rue de la papeterie, 38402 St-Martin d'Hères, France
{adel.albaba,stephane.lambert,francois.nicot}@irstea.fr
[2] 3SR, UJF-INPG-CNRS-UMR5521, DU Grenoble Université, 38041 Grenoble, France
bruno.chareyre@inp-3sr.fr

Abstract. This paper presents a numerical model based on Discrete Element Method (DEM) used to reproduce a series of tests of dry granular flow. The flow was composed of poly-dispersed coarse-grained angular particles flowing in an inclined flume and interacting with a divided rigid wall. The normal impact force against the wall has been studied in details considering the force on each part of the wall. The model has been calibrated based on the flow thickness measurements. By quantitative comparison with experimental data, the model showed good agreement in terms of peak force on each part of the wall, the time of the peak and also the residual force values at the end of the tests.

Keywords: DEM, Granular flow, Obstacle, Impact, Numerical modeling.

1 Introduction

The urbanization of the mountainous areas raised the importance of mitigating the threats to people and infrastructures linked to natural hazards such as rockfalls and granular flows. Several catastrophic granular flow events (Fig. 1) happened in the past resulting in major catastrophes and large loss of lives.

Granular flows has been classified as one of the most hazardous landslides due to its high flow velocity and impact forces, long runout distance and poor temporal predictability [1]. More specifically, dry granular flows produced by shallow slope failures were found to travel long distances destroying infrastructures and blocking vital roads. In terms of formation, they contain large blocks of gravel and rock fragments.

Granular flows hazard can be limited using retention systems similar in principle to rockfall barriers [3]. Different protection structures have been proposed in the literature for the mitigation of natural hazards; they are mainly retaining walls or flexible structures. Retaining walls have been widely used in China and also in Japan [4] for the prevention of rockfalls and granular flows. For the same reason, different types of flexible structures using anti-submarine nets have been developed over the last decades [5,6].

W. Wu (ed.), *Recent Advances in Modeling Landslides and Debris Flows*,
Springer Series in Geomechanics and Geoengineering, DOI: 10.1007/978-3-319-11053-0_9

Fig. 1. Dry granular flow after Wenchuan earthquake, China [2]

Several researches have been carried out in order to model granular flows. On one hand, continuum treatment has often been adopted where flows characteristics are analyzed by the Eulerian forms of continuity and momentum equation [7,8,9].

On the other hand, with the use of a Discrete Element Method (DEM), Silbert et al. [10] carried out 2D and 3D simulations of mono-dispersed particles flowing in a chute in a steady-state condition where observations were taken regarding structure and rheology of the flow. DEM was also used to simulate a rock avalanche event that took place in Italy [11]. Faug et al. [12] proposed a hydrodynamic model based on depth-averaged momentum conservation which was used to predict DEM numerical results of a free-surface gravity-driven dense flow overflowing a wall.

On the experimental side, various experiments have been conducted ranging from studies on geological debris flows to well characterized laboratorial granular flows down an inclined plane [13], [8], [14]. Furthermore, Faug et al. [15] experimentally investigated the dead zone formation of glass beads behind an obstacle down an inclined channel. In addition, other DEM models were validated against small tests experiments in different slopes for better prediction of runout distances and impact force against obstacles [16].

However, none of the experiments considered coarse-grained flow of angular particles which is the main case for dry granular flow. To serve this purpose, Jiang and Towhata [2] recently studied the impact behavior of dry granular flow against a rigid retaining wall using poly-dispersed mixture of limestone gravel. Measurements of normal impact force vs. time were recorded along with observations of flow thickness and flow velocity.

The aim of this paper is to present a model capable of simulating the impact of dry coarse-grained flow against a rigid wall taking into account the shape effect of the angular particles. First, we will describe the model in terms of contact law, particles shape and flume characteristics. Afterwards, the model calibration and validation are presented with discussion of obtained results. Finally conclusions of the presented work are drawn.

2 Numerical Modeling

The numerical simulation of the dry granular flow was carried out using Discrete Element Method. Nowadays DEM is widely used for modeling granular media. It is particularly efficient for static and dynamic simulation of granular assemblies where medium can be described at a microscopic scale. The method is based on the molecular dynamics approach proposed by Cundall and Strack [17].

In comparison with Finite Element Method (FEM), DEM makes large displacements between elements easy to simulate. In addition, DEM surpasses FEM when dealing with discontinuous problems where FEM becomes computationally demanding [18].

YADE software has been used as a modeling tool which is an extensible open-source framework for discrete numerical models, focused on Discrete Element Method [19].

2.1 Contact Law

A visco-elastic contact law with Mohr-coulomb failure criterion (Fig. 2) has been adopted where normal and tangential contact forces F_n, F_t between particles were calculated as follows:

$$\overrightarrow{F_n} = (k_n\, u_n - \gamma\, \dot{u_n})\, \vec{n} \tag{1}$$

$$\overrightarrow{F_t} = \begin{cases} \frac{k_t\, \overrightarrow{u_t}}{|k_t\, \overrightarrow{u_t}|} \left|\overrightarrow{F_n}\right| \tan\varphi & if\ |k_t\, \overrightarrow{u_t}| > \left|\overrightarrow{F_n}\right| \tan\varphi, \\ k_t\, \overrightarrow{u_t} & otherwise \end{cases} \tag{2}$$

Where k_n and k_t are the normal and tangential stiffness parameters, u_n and u_t are the normal and shear displacements, $\tan\varphi$ is the friction coefficient and γ is the viscous damping coefficient. k_t was taken as $(2/7)k_n$ according to what was previously suggested by [10].

Based on Schwager and Pöschel [20], with the restitution coefficient (ε) being the ratio between velocities after and before the impact, It can be calculated as follows:

$$\omega_0^2 = \frac{2k}{m_{eff}} \tag{3}$$

$$\beta = \frac{\gamma}{m} \tag{4}$$

$$\omega = \sqrt{\omega_0^2 - \beta^2} \tag{5}$$

$$\varepsilon = \frac{\dot{u}(t_c^0)}{\dot{u}(0)} = e^{-\beta\, \pi/\omega} \tag{6}$$

Where $m_{eff} = (1/m_1 + 1/m_2)$ and $\dot{u}(t_c^0)$, $\dot{u}(0)$ are velocities after (at the end of the contact) and before the collision respectively.

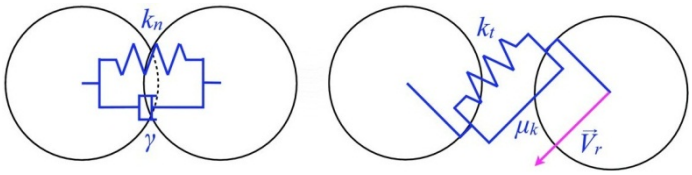

Fig. 2. Normal and tangential interaction forces of the contact [21]

It is worth noting that, in the current study, the tangential viscous damping coefficient has been set to zero (using ε_t = 1.0). This is due to the absence of lubricated contact (as we are dealing with a dry flow), which is usually the proposed physical explanation for accounting for tangential viscous damping coefficient [22]. Particle stiffness k_{par} = E D/2 where E is the Young's modulus (taken as 10^8 Pa) and D is the particle diameter. In order to ensure rigidity, the wall stiffness was taken ten times the stiffness of D_{50} particle. The value of ε was calibrated in Section 3 considering the flow thickness measurements.

2.2 Flowing Particles, Clumping and Shape Effects

Particles in use were of a poly-dispersed mixture with with D_{50} of the model being 15 mm and ranging from 10 mm to 20 mm in diameter with an average friction angle of 53˚ (similar to the one used in [2]). With the aim of simulating angular gravels, a two-spheres clump particle was used which has great advantageous in: controlling rotational velocity, adding interlocking effect between particles and improving shape representation of the angular gravel (section 3.1). Furthermore, the simulation is kept rather inexpensive (with the use of only two particles for forming the clump). The clump consists of two identical spheres (with a radius R) overlapping over a distance R thus having an aspect ratio of $\frac{3}{2}$ R.

2.3 Sample Preparation

The samples were prepared in a box with varying lengths (from 14 cm to 44 cm with a 5 cm step) and heights (from 5 cm to 20 cm with a 5 cm step) but with a 30 cm fixed width. The samples were released in a dam-break manner in which the gate was pulled up rapidly and instantaneously. With the total weight of the sample being equal to the weight of a single D_{50}-sphere multiplied by the number of particles, the number of generated particles (num) was calculated as follows:

$$num = \left(\frac{V_t\,\gamma_t}{V_s\,\gamma_s}\right) \tag{7}$$

where V_t is the total volume of the sample, γ_t is the specific weight of the sample (13.5 kN/m^3), V_s is the volume of a single D_{50}-sphere and γ_s is the specific weight of gravel particles (taken as 26.5 kN/m^3 for the limestone gravel considered). Afterwards, each spherical particle was replaced with a clump consisting of two equal

spheres. Radii of clumped-spheres were calculated so that the mass and volume of the clump is equal to that of the particle which it replaces.

2.4 Modeling of the Experimental Set Up

The flume dimensions were based on the experimental flume used by [2]. The flume was rectangular in cross section with 219 cm length, 30 cm width and 35 cm height. Different inclination angles α were tested ranging from 35˚ to 45˚. The friction angle specified to the flume base, flume sides and the rigid wall were 25˚, 15˚ and 21˚ respectively. A frictionless triggering gate was used to initiate the flow. At the end of the flume, a perpendicular rigid wall divided into six horizontal segments (marked from 1 to 6 starting from the bottom) was used. Interaction forces were recorded with each 5-cm height segment of the wall. No overflowing (topping) of the wall took place in all tests.

3 Model Calibration

With our aim being modeling granular flow of angular particles, experimental data [2] has been selected for our model calibration. Three different tests have been carried out: Test L34-H15-α45°, Test L44-H15-α40° and Test L44-H20-α40°. For instance, Test L44-H15-α40° represents a sample having 44 cm in length, 15 cm in height and 40˚ inclinational angle.

3.1 Clumps vs. Spherical Particles

A comparative study is presented showing the effect of using the clumps on capturing the shape effect of the angular particles. Two samples were tested the first having spherical particles and the second having clumped ones. The chosen clump has a lower rotational energy in comparison with the spherical particle (Fig. 3a) resulting in a denser flow. Furthermore, the final shape of the deposit is closer to reality with the clumped particle case in comparison with the spherical one. Consequently, compared with the spherical particles, peak and residual values (Fig. 3b) on the sixth segment of the wall for clumped particles are closer to the experimental (experimental values: $F_{peak} \approx 14$ N/m, $F_{res} \approx 10$ N/m). This might be due to the rolling resistance provided by the clump shape which prevents the particles from rolling over the dead zone deposit and accumulate behind part 6 of the wall.

3.2 Flow Thickness and Velocity

The measurements of flow thickness and velocity were considered at the time where the total force on the wall reaches its maximum value in order to be comparative with the experimental data (as done in the experiment). The targeted part of the flow for calculating velocity and thickness were particles within a distance ranging from 40 to 50 cm away from the wall. However, since the flow has two regimes along the flow

thickness-collisional and frictional- cumulative frequency were drawn in which thickness and velocity values were taken at 90% of total frequency. A value of $D_{50}/2$ was added to 90% cumulative frequency of the flow thickness to account for the free surface of the flow.

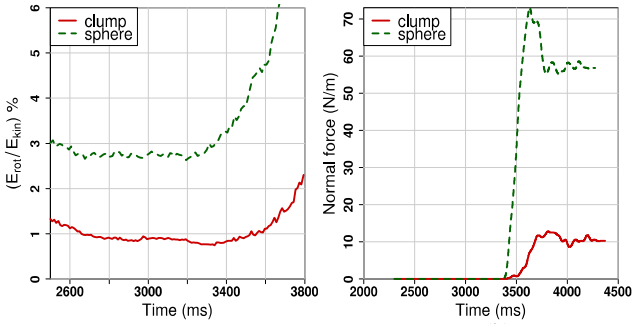

Fig. 3. (a) Ratio of rotational energy to total kinetic energy for clumps and spheres, (b) Normal force on part 6 of the wall

Different values of restitution coefficient were tested and flow thickness values were observed for each corresponding restitution coefficient. It was found that ε = 0.3 is suitable for our flow based on flow thickness measurements resulting in a model value of 3.9 cm which well-correspond to the experimental value of 3.9 cm (Fig. 4a).

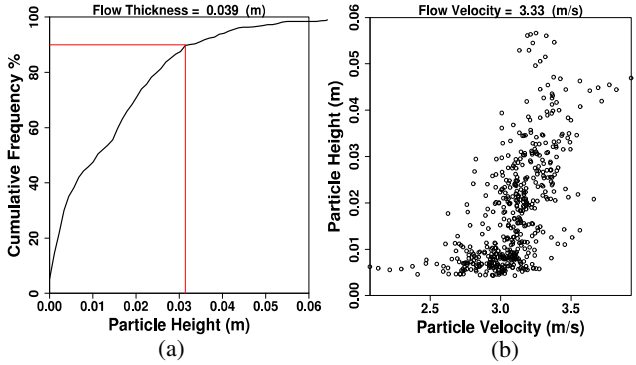

Fig. 4. (a) Cumulative frequency of gravity center of particles height, (b) Variation of particles velocity with heights

However, velocity measurements of test L44-H15-α40° in the model (Fig. 4b) taken at the considered flow thickness (at 90% for cumulative frequency) was found to be lower than experimental value (4.13 m/s) which still needs improvement. Above all, features of granular flow have been observed by the model showing a dilute front followed by a denser part (Fig. 5).

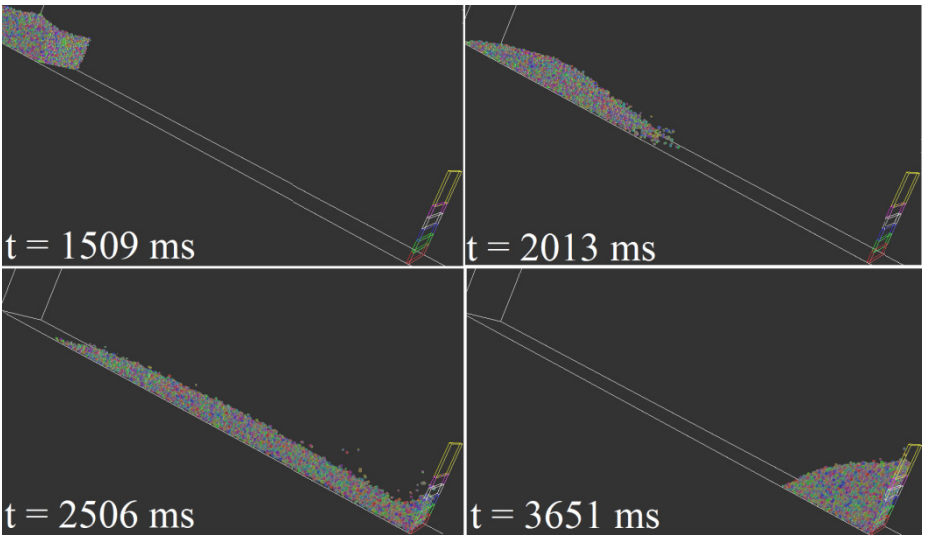

Fig. 5. 3D view of the evolution of simulated flow through time, test L44-H20-α40°

4 Model Validation

The rigid wall response against the granular flow impact has been investigated in details. Indeed, special attention has been given to the normal force applied on each part of the rigid wall where curves of normal impact force vs. time were analyzed. Data treatment was carried out using smooth spline method where a smooth curve is fitted to a set of noisy data using spline function [23].

4.1 Test L34-H15-α45°

In this test (Fig. 6a), the sample had 34 cm length, 15 cm height and 45° inclinational angle. On the first element of the wall (F_1), the peak force was found to be 396 N/m which is fairly close to the experimental value (around 350 N/m). Moreover, the time of the peak force F_1 is relatively similar to the experiment with a value around 3676 ms but with a lower residual force in the model (145 N/m) compared with the experiment (175 N/m) which might be due to the force chain distribution and particles shape arrangement behind the wall. Likewise, in contrast to F_1, the peak value of F_2 in the model (256 N/m) was lower than the experimental value (300 N/m). For F_3 and F_4, the model captured the peak time of forces fairly well (being 3883 and 3994 ms for F_3 and F_4 respectively) but with a lower peak value. The peak force and timing of the peak on F_5 and F_6 were fairly captured by the model along with their residual force values.

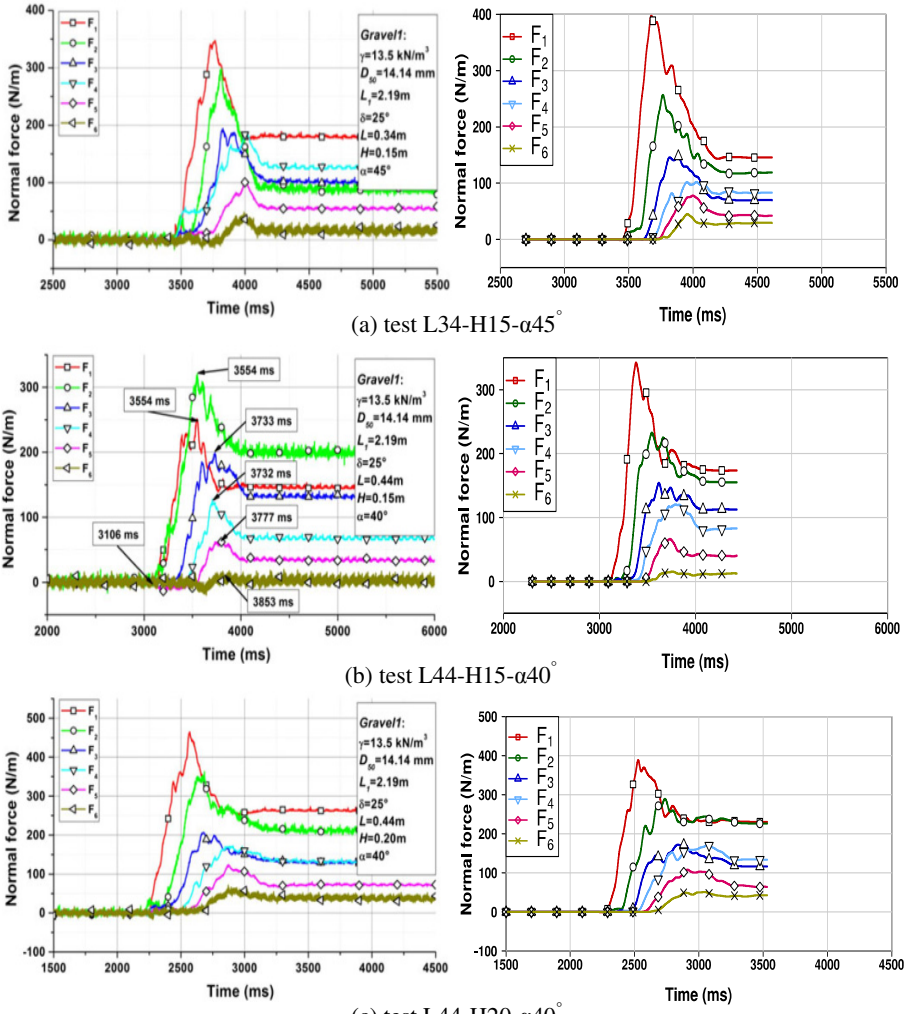

Fig. 6. Time history of normal force variation: experiment (left) [2] and model (right)

4.2 Test L44-H15-α40°

For this test, the model recorded peak impact force values of 341 and 232 N/m for F_1 and F_2 respectively (Fig. 6b). Compared to the experiment, similar values were observed but with a reversed order ($F_2 > F_1$). According to [2], this might be due to an arching effect forming an arch-like protective layer on part 1 of the wall resulting in a non-linear distribution of force with depth. Such a layer is also thought to affect the residual force values of F_1 and F_2. Concerning the rest parts of the wall, the model managed to capture the peak forces of F_3, F_4, F_5 and F_6 (with a small exception for F_3) with values of 154, 120, 66 and 15 N/m respectively along with peak times 3619,

3808, 3733 and 3761 ms respectively. Residual forces on these parts were found to be 112, 82, 40 and 12 N/m respectively which are close to the experimental observations. In terms of total normal force (Fig. 7), the model fairly agrees with the experiment in terms of the peak force (735 N/m), peak time (3733 ms) and residual total force (576 N/m).

4.3 Test L44-H20-α40°

With the use of higher volume of the sample, the trend of the impact force curves was better captured with the model along with the time lag between each force curve. For instance, F_1 peaks at 2523 ms with a value of 387 N/m (450 N/m in the experiment) which is followed by another flow surge leading F_2 to peak with 288 N/m (340 N/m in the experiment) at 2737 ms. Residual forces of F_1 and F_2 were found to be similar to the experiment with values of 227 and 226 N/m respectively. Very good agreement has also been observed for F_3, F_4, F_5 and F_6 in terms of peak forces (172, 172, 108 and 51 N/m) the time of the peak (2864, 3070, 2912 and 3043 ms) and residual force values (116, 134, 65 and 43 N/m). Above all, to some extent, arching was managed to be captured in this test, especially for residual forces of F_1-F_2 and F_3-F_4. This might be due to the higher volume of the sample used in this test in comparison with previous tests which permitted better representation of the experiment as larger number of particles is used.

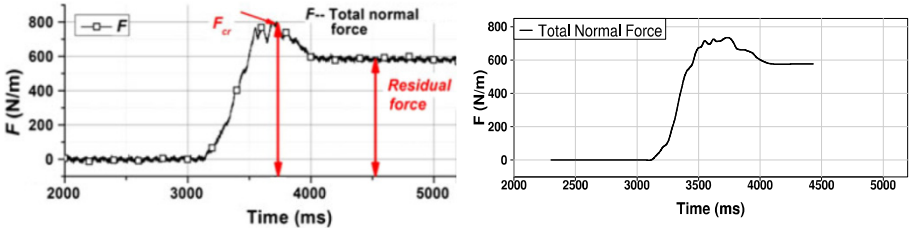

Fig. 7. Time history of total normal force variation, test L44-H15-α40°: experiment (left) [2] and model (right)

5 Conclusions

In this paper, we have numerically studied the impact of granular flow against a rigid wall considering clumped particles. The proposed model has shown capabilities of capturing the main features of normal impact force against a rigid wall. Good agreement has been observed in terms of the peak force on each part of the wall, the time of the peak and the residual force at the end of the test. Moreover, to some extent, the model was able to account for the arching that was observed in the experiment.

Furthermore, the model shows collisional regime in the shallow layer and frictional regime in the deeper ones. The use of clumps was found to be beneficial for accounting for the shape effects caused by sharp angles of coarse-grained particles. It was shown that the use of clumped particles is preferred over the spherical particles in

controlling rotational velocity where it was reduced by 70 % with the use of clumps. Indeed, the shape of the deposition behind the wall was improved by the clumped particles leading to a force distribution which is closer to the experimental values. After being validated against rigid walls, the wall in the model will be replaced by flexible structure (net elements) in which the impact behavior will be studied in details.

Acknowledgment. The research leading to these results has received funding from the People Programme (Marie Curie Actions) of the European Union's Seventh Framework Programme FP7/2007-2013/ under REA grant agreement n° 289911.

References

1. Jakob, M., Hungr, O.: Debris-flow Hazards and Related Phenomena. Springer, Heidelberg (2005)
2. Jiang, Y., Towhata, I.: Experimental Study of Dry Granular Flow and Impact Behavior against a Rigid Retaining Wall. Rock Mechanics and Rock Engineering 46(4), 713–729 (2013)
3. Guasti, G., Volkwein, A., Wendeler, C.: Design of Flexible Debris Flow Barriers. In: Genevois, R., Hamilton, D.L., Prestininzi, A. (eds.) 5th International Conference on Debris-Flow Hazard "Mitigation, Mechanics, Prediction and Assessment", Padua, Italy, June 14-17, pp. 1093–1100. Casa Editrice Università La Sapienza, Rome (2011)
4. Kishi, N., Ikeda, K., Konno, H., Kawase, R.: Prototype Impact Test on Rockfall Retaining Walls and its Numerical Simulation. In: Proceedings of Structures under Shock and Impact IV, Cambridge, England, pp. 351–360 (2000)
5. Nicot, F., Cambou, B., Mazzoleni, G.: Design of Rockfall Restraining Nets from a Discrete Element Modeling. Rock Mechanics and Rock Engineering 34(2), 99–118 (2001)
6. Volkwein, A.: Numerical Simulation of Flexible Rockfall Protection Systems. In: Proceedings of the International Conference on Computing in Civil Engineering, Cancun, Mexico, July 12-15, p. 11. ASCE (2005)
7. Hutter, K., Koch, T., Plüss, C., Savage, S.B.: The Dynamics of Avalanches of Granular Materials from Initiation to Runout. Acta Mechanica 109, 127–165 (1995)
8. Azana, E., Chevor, F., Moucheront, P.: Experimental Study of Collisional Granular Flows down an Inclined Plane. Journal of Fluid Mechanics 400, 199–227 (1999)
9. Pudasaini, S.P., Hutter, K.: Rapid Shear Flows of Dry Granular Masses down Curved and Twisted Channels. Journal of Fluid Mechanics 495, 193–208 (2003)
10. Silbert, L.E., Erta, S.D., Grest, G.S., Halsey, T.C., Levine, D., Plimpton, S.: Granular Flow Down an Inclined Plane: Bagnold Scaling and Rheology. Physical Review E 64, 051302 (2001)
11. Calvetti, F., Crosta, G., Tatarella, M.: Numerical Simulation of Dry Granular Flows: From the Reproduction of Small Scale Experiments to the Prediction of Rock Avalanches. Rivista Italiana di Geotecnica 21(2), 1–38 (2000)
12. Faug, T., Beguin, R., Benoit, C.: Mean Steady Granular Force on a Wall Over-flowed by Free-surface Gravity-driven Dense Flows. Physical Review E 80, 021305 (2009)
13. Campbell, C.S., Cleary, P.W., Hopkins, M.: Large-scale Landslide Simulations: Global Deformation, Velocities and Basal Friction. Journal of Geophysical Research 100(B5), 8267–8283 (1995)

14. Lemieux, P.A., Durian, D.J.: From Avalanches to Fluid Flow: a Continuous Picture of Grain Dynamics Down a Heap. Physical Review Letters 85, 4273–4276 (2000)
15. Faug, T., Lachamp, P., Naaim, M.: Experimental Investigation on Steady Granular Flows Interacting With an Obstacle Down an Inclined Channel: Study of the Dead Zone Upstream From the Obstacle. Application to Interaction between Dense Snow Avalanches and Defense Structures. Natural Hazards and Earth System Sciences 2, 187–191 (2002)
16. Valentino, R., Barla, G., Montrasio, L.: Experimental Analysis and Microme-chanical Modeling of Dry Granular Flow and Impacts in Laboratory Flume Tests. Rock Mechanics and Rock Engineering 41(1), 153–177 (2008)
17. Cundall, P.A., Strack, O.D.L.: A Discrete Numerical Model for Granular Assemblies. Géotechnique 29, 47–65 (1979)
18. Bertrand, D., Trad, A., Limam, A., Silvani, C.: Full-Scale Dynamic Analysis of an Innovative Rockfall Fence Under Impact Using the Discrete Element Method: from the Local Scale to the Structure Scale. Rock Mechanics and Rock Engineering 45(5), 885–900 (2012)
19. Šmilauer, V., Catalano, E., Chareyre, B., Dorofeenko, S., Duriez, J., Gladky, A., Kozicki, J., Modenese, C., Scholtès, L., Sibille, L., Stránský, J., Thoeni, K.: Yade Documentation. In: Šmilauer, V. (ed.) The Yade Project, 1st edn. (2010), http://yade-dem.org/doc/
20. Schwager, T., Pöschel, T.: Coefficient of Restitution and Linear–dashpot Model Revisited. Granular Matter 9(6), 465–469 (2007)
21. Sánchez, P., Scheeres, D.J.: Simulating Asteroid Rubble Piles with a Self-gravitating Soft-sphere Distinct Element Method Mode. The Astrophysical Journal 727(2), 120–133 (2011)
22. Ghaisas, N., Wassgren, C.R., Sadeghi, F.: Cage Instabilities in Cylindrical Roller Bearings. Journal of Tribology 126, 681–689 (2004)
23. Chambers, J.M., Hastie, T.J.: Statistical Models in S. Wadsworth & Brooks/Cole, Pacific Grove (1992)